A THREE-DIMENSIONAL PHOTOCHEMICAL-TRANSPORT MODEL OF THE MARTIAN ATMOSPHERE. F. Lefèvre, *Service d'Aéronomie, CNRS/Univ. Paris 6, 75252 Paris Cedex 05, FRANCE, (franck.lefevre@aero.jussieu.fr)*, S. Lebonnois, F. Forget, *Laboratoire de Météorologie Dynamique, CNRS/Univ. Paris 6, 75252 Paris Cedex 05, FRANCE*.

Introduction

This paper presents preliminary results of the first three dimensional simulations of the Martian photochemistry. Up to now only one-dimensional models (e.g., [1], [2], [3], [4]) have generally been used to determine the vertical profiles of trace constituants in the Mars atmosphere. These models have been very useful to estimate the globally averaged distribution of chemical species as a function of height, and have emphasized the role of water vapor to explain the classical problem of the stability of the Martian CO_2 atmosphere. However, one-dimensional models cannot represent the dramatic meridional variations of the distribution of trace species caused by the usually strong pole-to-pole gradient of atmospheric temperature and water vapor. The effects of the meridional transport of chemical species are also ignored, and a highly uncertain eddy diffusion coefficient is used to represent the vertical transport and mixing. The only two-dimensional simulations published by *Moreau et al.* [5] provided a better description of the interaction between dynamics, radiation, and chemistry, although the model did not include a consistent representation of the water cycle nor a treatment of the dynamics near the surface where the topographical effects are important.

In the present work, a new chemical model of the Martian atmosphere has been coupled to the general circulation model (GCM) developed at LMD for the last 10 years [6]. Trace constituents are tranported by the three-dimensional winds and convective processes calculated by the GCM. Their chemical evolution is computed by the chemical module as a function of the pressure and temperature fields, solar zenith angle, heliocentric distance, and the amount of water vapor, which is also affected by condensation and sublimation processes. The evolution of the chemical species is therefore computed in three dimensions over the Martian globe and is fully interactive with the GCM dynamics, radiation field, and water cycle. Presently, we use a rather low horizontal resolution ($11.25^\circ \times 7.5^\circ$), with 32 vertical layers, from the surface up to 120 km.

The photochemical module

The first version the chemical model used in the present work describes the chemistry of oxygen, hydrogen, and CO. Eleven species are taken into account and individually transported by the coupled model (O, $O(^1D)$, O_2, O_3, H, OH, HO_2, H_2O_2, H_2, H_2O, CO). Photolysis rates are calculated from the model of *Madronich and Flocke* [7] adapted to the Martian conditions. Calculations are performed off-line at high spectral resolution (0.1 nm), in spherical geometry, and take into account the vertical distribution of CO_2, H_2O, O_2, and O_3 to determine the atmospheric opacity in the UV region. The most recent absorption cross-section datasets were used and include temperature dependence for CO_2, O_2, O_3, and H_2O_2. Once calculated from 0 to 95° the vertical profiles of photolysis rates are stored in a three-dimensional lookup table as a function of the solar zenith angle and the slant columns of CO_2 and O_3. At each chemical time step of the coupled model, the actual photolysis rate for each sunlit gridpoint is retrieved by interpolating the value inside the lookup table. Gas-phase reaction rate coefficients were in general taken from *Sander et al.* [8]. Rate coefficients of three-body reactions are increased by a factor of 2.5 to account for the higher efficiency of CO_2 as a third body in comparison with N_2 and O_2. Temperature and pressure values used to compute the reaction rates are provided for each grid point by the GCM. In order to reduce the computational cost of the integration, a family approach was adopted (O_x = O + O_3; HO_x = H + OH + HO_2), and photochemical equilibrium is assumed for O_3, $O(^1D)$, OH, and HO_2. The chemical evolution of long-lived species (O_2, H_2, H_2O, H_2O_2 and CO) and chemical families is solved by the iterative method described by *Shimazaki* [9].

Hydrogen peroxyde cycle

Hydrogen peroxyde, H_2O_2, is an important product of the odd-hydrogen chemistry in the Martian atmosphere. Being a very strong oxidizing species, it has been suggested that H_2O_2 might be responsible for the absence of organic compounds on the surface [10]. In addition to the large intensities of several of its fundamental bands in the infrared, H_2O_2 is predicted by the models to be the most abundant HO_x species near the surface, and should therefore be certainly less difficult to measure remotely than OH or HO_2. However, observations have so far failed to detect H_2O_2 in the Martian atmosphere. Recently *Encrenaz et al.* [11] could derive from their observations an upper limit for the H_2O_2 vertical column of $9\text{x}10^{14}$ to $1.2\text{x}10^{15}$ cm^{-2} which appears to be considerably lower than the estimates of previous 1D model simulations. We will report here preliminary results of the first 3D simulations of hydrogen peroxyde on Mars, and will compare the obtained values to the upper limit given by *Encrenaz et al.* [11].

Atmospheric hydrogen peroxyde is mainly formed by the reaction involving two HO_2radicals:

$$HO_2 + HO_2 \rightarrow H_2O_2 + O_2$$

HO_2 is a indirect product of the H_2O photolysis and therefore a strong correlation is expected between the water vapor and hydrogen peroxyde abundances. The main H_2O_2 loss mechanism occurs by photolysis:

$$H_2O_2 + h\nu \rightarrow OH + OH$$

with a characteristic time of about 6 hours in the lower atmosphere. H_2O_2 has therefore a much longer lifetime than

H, OH, and HO_2, and has no loss mechanism at night. This implies that photochemical equilibrium cannot be assumed in a model including the diurnal cycle. This species is individually integrated and transported in our model. Another important process included in the model is the condensation of H_2O_2, which may occur in the regions of very low temperatures. The calculated number densities are constrained to lie at or below the local saturation number density given from the expression by *Lindner* [12].

Fig. 1 displays the seasonal evolution of the H_2O_2 and H_2O column density zonal means. As expected hydrogen peroxyde is clearly correlated with the amount of water vapor available to produce HO_x radicals by photolysis. A strong seasonal variability of H_2O_2 is calculated by the model: the column abundance varies by a factor larger than 10 at high latitudes and a factor of about 3 at low latitudes, in phase with the water vapor changes caused by condensation, sublimation, and transport processes. Interestingly the maximum amount of H_2O_2 ($1.8x10^{16}$ mol cm^{-2} in late fall at 20N) does not correspond to the absolute maximum of water vapor, reached at the end of northern spring at high latitudes (about 100 precipitable microns), in good agreement with the observations. Examination of the evolution of the vertical distribution of H_2O at the Equator (Fig. 3) reveals that the hydrogen peroxyde maximum calculated near aphelion is a consequence of the variation of the saturation altitude of water vapor, leading to the production of large amounts of HO_x radicals over a domain of altitude almost twice as high as during the rest of the year.

Fig. 2 shows the calculated H_2O_2 vertical column at the same solar longitude (L_s = 112) when *Encrenaz et al.* [11] derived their upper limit of $9x10^{14}$ to $1.2x10^{15}$ cm^{-2} in the northern hemisphere. The model distribution shows a strong hemispheric contrast, linked to the abundance of water vapor which is maximum in the northern hemisphere at this time of the year. The topography also plays a significant role in the longitudinal and latitudinal variations of H_2O_2, as shown by the absolute maximum reached in the Utopia Planitia basin, whereas lower amounts are calculated at the same latitude over regions of higher elevation. Overall the quantities given by the model are larger than the upper limit by a factor 5 to 15. Several possible reasons for this overestimation are currently under investigation: the large uncertainties existing on crucial processes such as the H_2O photolysis in the Martian conditions, the choice of the rate constants of some key reactions involving OH or HO_2, as well as the possible loss of HO_x radicals to the surface of Mars. The results of sensitivity studies on these different parameters will be presented during the conference.

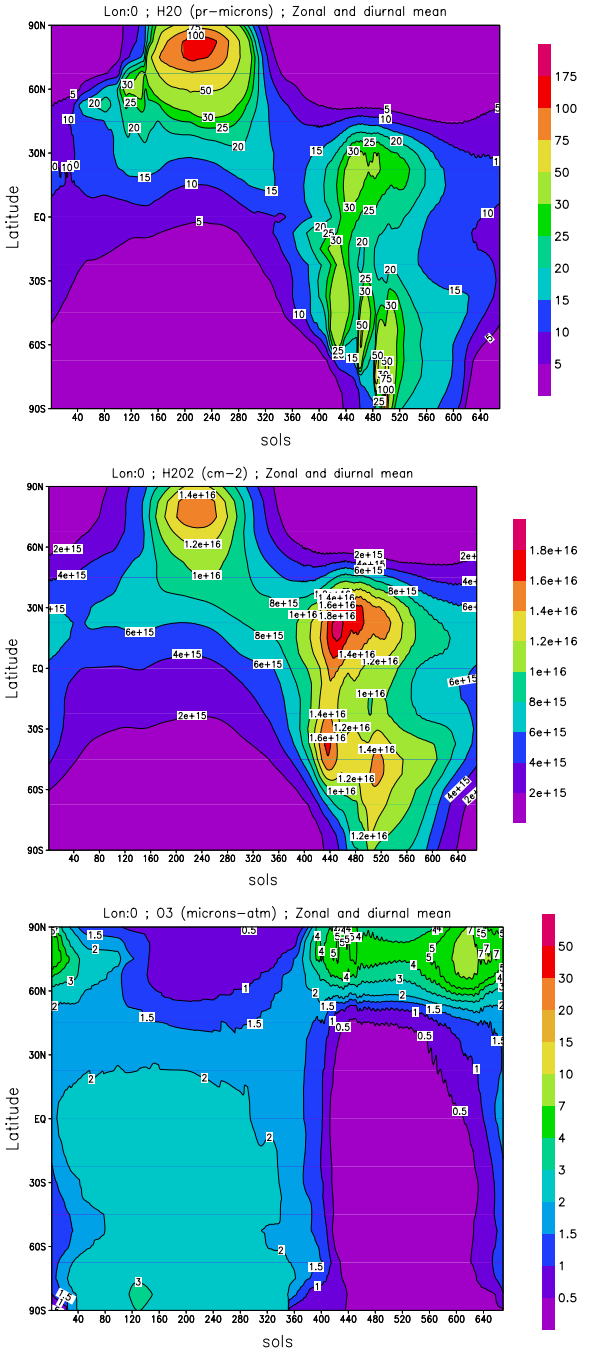

Figure 1: Seasonal cycles of water, hydrogen peroxyde and ozone: zonal and diurnal mean column densities as a function of latitude and days counted from northern spring equinox.

Ozone cycle

Atomic oxygen is produced in Mars atmosphere through the photodissociation of CO_2. It recombines to form molecular oxygen, and then ozone. Ozone is lost through photolysis, and through the reaction with HO_x radicals (OH, HO_2). Therefore, it is expected to be in strong anticorrelation with water vapor. As seen previously, it seems that our model overpredicts the abundance of these radicals. It is therefore not surprising that when we compare the distribution of ozone obtained in the model with available observations of ozone column densities ([13], [14], [15]), it seems that our model underpredicts ozone concentrations by a factor 2 to 5. Nevertheless, this three

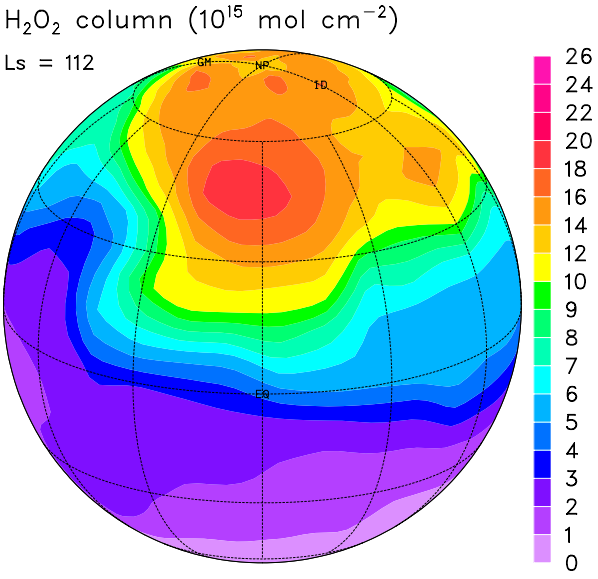

Figure 2: instantaneous H_2O_2 column (10^{15} molecule cm^{-2}) distribution calculated at L_s = 112. The observer is facing the meridian at 120W longitude (local time = 8PM).

dimensional model allows a close study of the seasonal and diurnal variations of ozone and other related chemical species, in relation with the water cycle. We will develop here some first examples of the possibilities of this tool.

The seasonal evolution of the ozone column density is shown in Fig. 1, together with water vapor and hydrogen peroxyde. The anticorrelation is clear, but the asymmetry between the southern and northern winters must be noted: related anticorrelations between ozone and water vapor are strongest for northern winter. This asymmetry is linked to the hygropause altitude, which varies significantly as a function of season, in correlation with the variations of the distance to the sun (aphelion around southern winter solstice, and perihelion around northern winter solstice) and with the dust load of the atmosphere (which has an impact on temperature). These variations are shown at equator in Fig. 3, for water vapor and ozone mixing ratios.

The diurnal cycle of ozone also displays remarkable seasonal (L_s) variations. To illustrate this, Fig. 4 shows maps of ozone column density at two opposite seasons: southern winter and northern winter solstices. In southern winter, ozone abundance is larger on the night side than on the day side, and therefore exhibits a strong diurnal cycle, with a clear footprint of the terminator. At the opposite season, the behavior is very different. The ozone abundance is much lower on almost all the planet, except around the winter pole, and no diurnal cycle is visible. These differences are linked to the global abundance of the HO_x radicals, in relation with the water vapor seasonal cycle. In the Northern winter polar vortex, condensation of water vapor on the surface suppresses the source of HO_x, leading to large O_3 maximum in good qualitative agreement with the observations. At all other latitudes, the increase

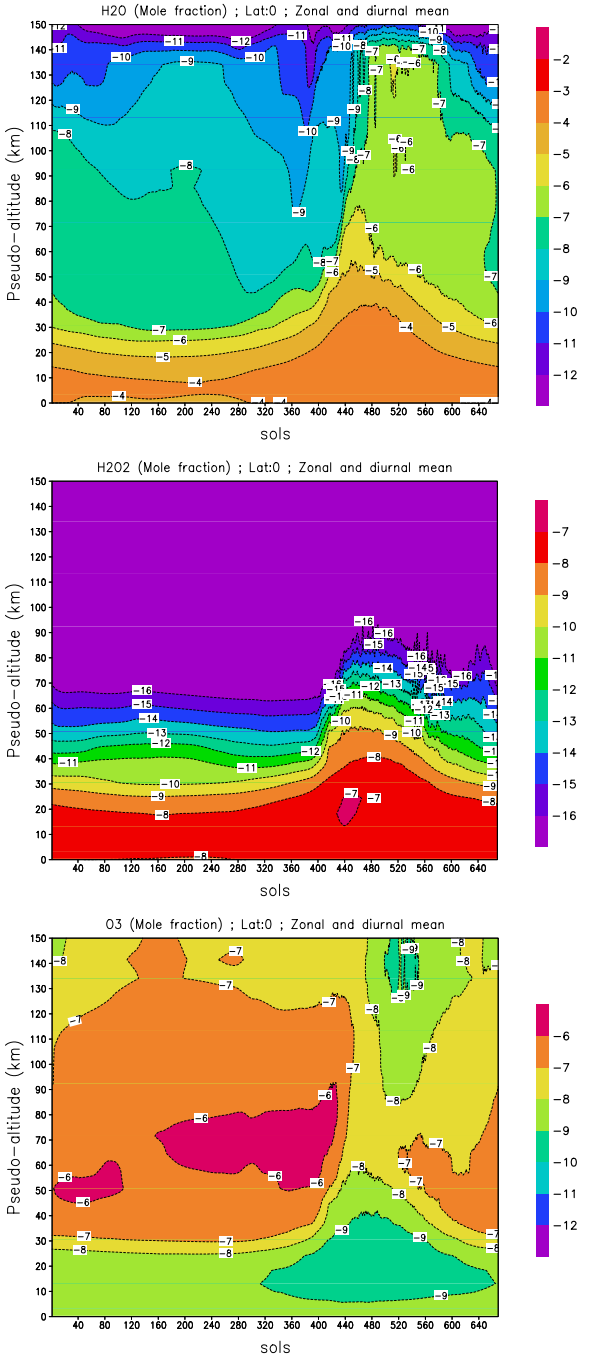

Figure 3: Seasonal variations of water vapor, hydrogen peroxyde and ozone at equator: zonal and diurnal mean mixing ratios (log) as a function of altitude and days counted from northern spring equinox.

of water vapor and the uprise of the hygropause calculated by the model near perihelion is responsible for the increased loss of O_x species by the HO_x radicals and the disappearance of

the ozone diurnal cycle.

Conclusion

We have developed the first three-dimensional photochemical-transport model of the Martian atmosphere. A photochemical module including 11 species and 38 photochemical reactions has been coupled to the LMD-GCM. Despite our use of the most recent photochemical data, the model appears to overestimate the abundance of hydrogen peroxyde and in the same time, to underestimate the observed ozone column density. These biases suggest that the amount of HO_x is too large in the model or/and the HO_x chemistry is too efficient at destroying odd oxygen. We plan to investigate carefully the reasons for this discrepancy, by analyzing the various sources of uncertainties in the currently recommended reaction rate coefficients and in our knowledge of absorption cross-sections of CO_2 and H_2O in the Mars conditions.

Nevertheless this new generation of model allows detailed studies of the spatial, seasonal and diurnal behavior of the composition of the Martian atmosphere. It will be applied to the analysis of the data of the SPICAM instrument onboard Mars-Express, for which stringent tests of our quantitative understanding of the Martian photochemistry will be possible by the comparison of the model results to the simultaneous observations of ozone and water vapor.

In the following months, we will improve the model along the following lines:

- the model resolution will be increased,
- the transport scheme for the water ice clouds developed for the LMD-GCM by Franck Montmessin will be taken into account to improve the water cycle,
- dust will be included in the UV radiative transfer calculations,
- nitrogen compounds will be added,
- interactions with the surface will be investigated,
- our photochemical model will be coupled with the version of the LMD-GCM extended to the thermosphere, developed by Monica Angelats-i-Coll.

References

[1] Parkinson, T.D., and D.M. Hunten, J. Atmos. Sci., 29, 1380-1390, 1972. [2] McElroy, M.B., and T.M. Donahue, Science, 177, 986-988, 1972. [3] Krasnopolsky, V.A., Icarus, 101, 313-332, 1993. [4] Nair, H., et al., Icarus, 111, 124-150, 1994. [5] Moreau, D., L.W. Esposito, and G. Brasseur, J. Geophys. Res., 96, 7933-7945, 1991. [6] Forget, F., et al., J. Geophys. Res., 104, 24155-24176, 1999. [7] Madronich, S., and S. Flocke, in Handbook of Environmental Chemistry (P. Boule, ed.), pp. 1-26, Springer-Verlag, Heidelberg, 1998. [8] Sander, S.P., et al., JPL publication 02-25, 2003. [9] Shimazaki, T., Terra Scientific Publishing, Tokyo, 1985. [10] Klein, H.P., N.H. Horowitz, and K. Biemann, in Mars, University of Arizona Press, 1992. [11] Encrenaz, T., et al., Astronomy and Astrophysics, 396, 1037-1044, 2002. [12] Lindner, B.L., Planet Space Sci., 36, 125-144, 1988. [13] Espenak, F., et al., Icarus, 92, 252-262, 1991. [14] Clancy, R.T., M.J. Wolff, and P.B. James, Icarus, 138, 49-63, 1999. [15] Novak, R.E., et al., Icarus, 158, 14-23, 2002.

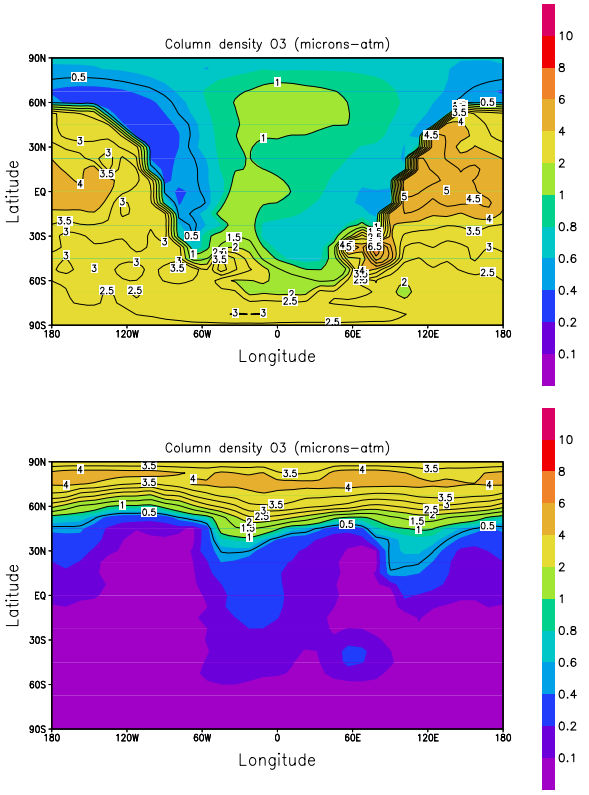

Figure 4: Instantaneous maps of column ozone (micron-atmosphere) for southern winter solstice (top) and northern winter solstice (bottom).